Numerical Investigation of Silicon Nitride Trench Waveguide

Qiancheng Zhao, Yuewang Huang, Rasul Torun, Shah Rahman, Tuva C. Atasever and Ozdal Boyraz*
Department of Electrical Engineering and Computer Science, University of California, Irvine, CA, USA, 92697.

*oboyraz@uci.edu

ABSTRACT

We numerically investigated optical properties, including evanescent intensity ratio (*EIR*), effective refractive index (N_{eff}), dispersion coefficient (*D*), and mode area (A_{eff}) of the silicon nitride trench waveguides fabricated by using conventional lithography. The waveguides are etched 3 μm deep with potassium hydroxide for triangle and trapezoidal waveguides, which is then followed by 3 μm thermal oxidation and 725 nm silicon nitride deposition. The waveguide with 725 nm thickness has an *EIR* peak of 0.025 when its bottom width W_{btm} equals 0.65 μm. A thinner waveguide has higher evanescent intensity ratio, which can be used in sensing applications. The locations of *EIR* peaks correspond to the quasi-TM and TE mode boundary. Narrower waveguides mainly support quasi-TM modes, whereas wider waveguides can support only TE modes. As the waveguide width increases, higher orders of TE modes emerge. In addition, a boundary of TE single mode and multimode can also be linearly curve fitted, according to the starting points of TE higher modes, in order to provide the single mode condition of the waveguide. The waveguide dispersion can be engineered to be in the anomalous region while at the same time remain close to zero. The waveguide with 725 nm thickness and 0.2 μm bottom width has its anomalous dispersion region between the wavelength of 1356 nm and 1462 nm. The mode area decreases with increasing waveguide width. This is the first time we have studied the mode properties of trench waveguides systematically. The waveguide will find more applications in sensing and nonlinear fields with the help of this mode analysis.

Keywords: numerical analysis, evanescent intensity ratio, single mode condition, dispersion, silicon nitride, trench waveguide.

1. INTRODUCTION

Silicon nitride has a broad transparency window ranging from the visible [1] to the mid-infrared. The moderate refractive index difference between silicon nitride and silicon dioxide, $\Delta n \approx 0.55$, makes the silicon nitride waveguide with silicon dioxide cladding suitable for low loss propagation [2]–[6]. In addition, Si_3N_4 waveguides are suitable for nonlinear applications [7] due to their high Kerr index [8] and their lack of two-photon-absorption and free-carrier-absorption [9] in the near infrared region. Nonlinear effects such as parametric frequency comb generation [9]–[11] and supercontinuum generation [12] have been demonstrated. On the fabrication side, silicon nitride can be deposited by standard CMOS fabrication technology, and experiments have already proven that silicon nitride, silicon dioxide and silicon components can be all integrated into one photonic device [13] to achieve complex modulation functionality [14].

We recently demonstrated a sub-micron silicon nitride trench waveguide using conventional photolithography with low propagation loss and high nonlinearity [6]. The fabricated waveguide has a propagation loss as low as 0.8 dB/cm and an impressive nonlinear refractive index $n_2 = 1.39\times10^{-19}$ m^2/W. The waveguide, buried in a trench valley, is an ideal platform for microfluidic sensing. However the evanescent field that extends outside the waveguide is usually weak. Therefore, nanoantennas can be employed to enhance evanescent wave-matter interaction. For optical trapping polystyrene nanobeads, we applied the trench waveguides with the help of bowtie antennas [15], and for nonlinear enhancement, we deposited the waveguide with gold nanoparticles [16].

Understanding the mode properties of the silicon nitride trench waveguide is of great significance to designing applications. The cross-section of our waveguide is irregular, with its core region in a triangle or trapezoidal shape. In

Photonic Fiber and Crystal Devices: Advances in Materials and Innovations in Device Applications IX, edited by Shizhuo Yin, Ruyan Guo, Proc. of SPIE Vol. 9586, 95860O · © 2015 SPIE
CCC code: 0277-786X/15/$18 · doi: 10.1117/12.2188378

the past, theoretical analysis based on FEM method [17], effective index method [18], Rayleigh principle and least-squared method [19], and weighted residual method [20] have been put forward to study the mode properties in trapezoidal waveguides. However, conclusions drawn from these analyses cannot be applied to our waveguide directly. Our waveguide differs from common rib trapezoidal waveguides because of the side walls, shown in FIG. 1. In general, the mode is horizontally guided by discontinuities of Si_3N_4 and vertically guided by index difference. But in some cases, the side walls connecting the bottom core region will induce light to leak into the slab region. Thus, specific analysis must be performed, which will be practically meaningful.

In this paper, We will first briefly introduce the fabrication procedure in Section 2. Then staring from the evanescent intensity ratio, we investigate the leakage of the waveguide, followed by quasi-TM and TE boundary study. The mode profile is studied and the TE single mode condition is put forward based in Section 3. Dispersion properties of the waveguides with different thicknesses are also studied for nonlinear applications, followed by a summary in Section 4.

2. TRENCH WAVEGUIDE FABRICATION

Recently, a novel approach of fabricating sub-micron silicon nitride trench waveguide by conventional lithography has been experimentally demonstrated [6]. Fabrication of the waveguide is rather straight forward and does not require E-beam lithography to achieve sub-micron waveguide dimension, and merely relies on optical lithography followed by anisotropic potassium hydroxide etching. The anisotropic potassium hydroxide (KOH) etching on <100> silicon wafer carves a trapezoidal or triangular trench with an angle of 54.7° with respect to the substrate surface. The shape of the waveguide is determined by etching depth H, opening window W_{open} and silicon nitride deposition thickness T. For example, if W_{open} is smaller than $\sqrt{2}H$, a V-groove will be carved out and the fabricated waveguide will be triangular in shape. On the contrary, if W_{open} is larger than that value, KOH will carve isosceles trapezoidal trench. The width of the lower edge of the waveguide can be estimated as $W_{btm} = W_{open} - \sqrt{2}H$.

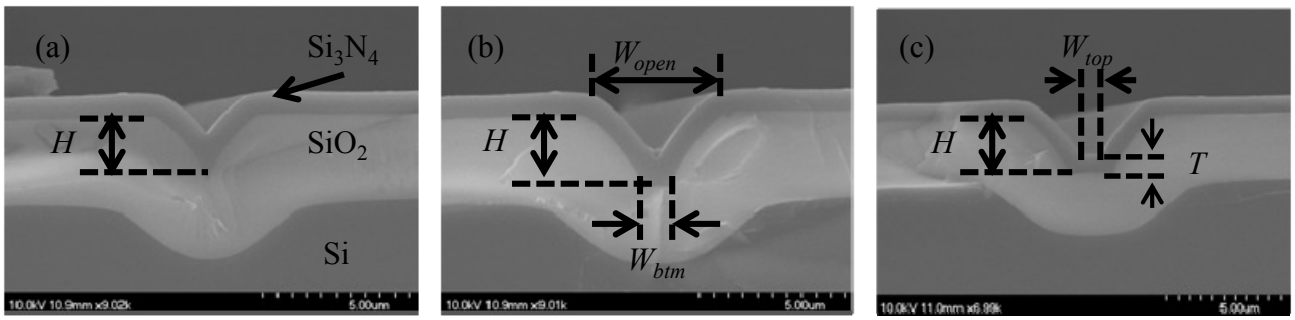

FIG. 1. SEM images for fabricated silicon nitride trench waveguides with thickness T = 725 nm, etching depth H = 3 μm, and top opening window (a) W_{open} = 4 μm, (b) W_{open} = 5 μm, and (c) W_{open} = 6 μm.

The W_{open} and H variables control the waveguide width, while the thickness of the waveguide is controlled by silicon nitride deposition. Low-pressure-chemical-vapor-deposition (LPCVD) was used to deposit a T = 725 nm layer of silicon nitride. The variation of the waveguide width and thickness affect the waveguide propagation properties and mode distributions. The waveguides propagation losses were experimentally measured using a cut-back method for both TE and TM modes [21]. Structure- and polarization-dependent propagation losses were summarized in Table I. We also experimentally tested the nonlinear refractive index n_2 of the guiding material to be 1.39×10^{-19} m^2/W. Further details can be found in Ref [6], [21].

Table I. Propagation loss of silicon nitride trench waveguide with different dimensions [21].

	TM	TE
W_{open} = 4 μm	1.66 ± 0.42 dB/cm	4.5 ± 0.34 dB/cm
W_{open} = 5 μm	0.8 ± 0.26 dB/cm	3.13 ± 0.37 dB/cm
W_{open} = 6 μm	6.43 ± 0.49 dB/cm	2.95 ±0.39 dB/cm

3. NUMERICAL ANALYSIS

To investigate the waveguide property thoroughly, we numerically analyzed waveguide in a FEM solver (COMSOL Multiphysics). The geometry of the structure, adopted from SEM images, is illustrated in FIG. 2. The side wall slope of the waveguide is 54.7°, consistent with wet etching properties. The connection between the Si_3N_4 side walls and top slabs is smoothened by Bezier curve. To reduce the variables in simulation, we fix the etching depth H to be 3.5 μm and disregard the opening window width W_{open}. Instead, the waveguide size is characterized by W_{btm} and T. In the simulation, the refractive index of the Si_3N_4 was measured using ellipsometry and curve fitted by Sellmeire equation as $n^2 = 1 + 3.585\lambda^2 / \left(\lambda^2 - 0.1316^2\right)$ [6], where λ is in the unit of μm. The refractive index of SiO_2 is adopted from [22].

The top cladding of the trench waveguide is air. Perfectly matched layer boundary conditions are used to minimize the back scattering at boundaries. All the simulations are performed at telecommunication wavelength 1550 nm unless otherwise specified.

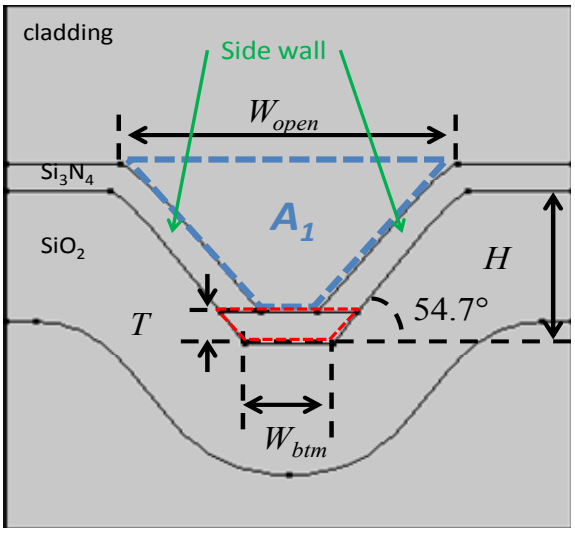

FIG. 2. Silicon nitride trench waveguide structure schematics. The region enclosed by the red dashed line is the waveguide core region. The region surrounded by the blue dashed line is the sensing region, and the area of this region is A_1. The total simulation area is denoted as A_{tot}.

3.1 Evanescent Intensity Ratio

The silicon nitride trench waveguide has an inborn advantage for microfluidic sensing, because the trench valley can work as container for liquids or gases. We have used the trench waveguide along with nanoantennas for plasmon optical trapping [15] and nonlinear enhancement [16] applications, in which evanescent fields from the bottom waveguide core region (enclosed by the red dashed line in FIG. 2) interact with analyte in the sensing region (enclosed by the blue dashed line in FIG. 2). The more evanescent field leaking into the sensing region, the more light-matter interaction there will be. To quantify the evanescent field strength, we define the evanescent intensity ratio as,

$$EIR = \frac{\iint_{A_1} \left|E(x,y)\right|^2 dxdy}{\iint_{A_{tot}} \left|E(x,y)\right|^2 dxdy} \tag{1}$$

where A_1 is the area of the trench channel and A_{tot} is the total simulation area that includes A_1. The EIR as a function of W_{btm} and T is plotted in FIG. 3(a). Thinner waveguides have higher EIR. Each curve has a peak and its peak location differs from those of the others. This profile is related with structure-dependent mode confinement. To be specific, the waveguide with T = 725 nm has its EIR peak of 0.025 when W_{btm} is close to 0.65 μm. When W_{btm} is below this value, the mode distribution is more TM dominant, which means the TM mode is tightly confined in the core region (FIG. 3(c)).

The extreme case is when W_{btm} equals 0, in which then the trapezoidal waveguide becomes a triangle waveguide. If W_{btm} is equal or wider than 0.65 μm, the mode distribution is more TE dominant (FIG. 3(d)). Correspondingly, TE mode is confined well as the waveguide gets wider. Near the peak location, neither the TM nor the TE mode are guided well, resulting in an increase in *EIR*.

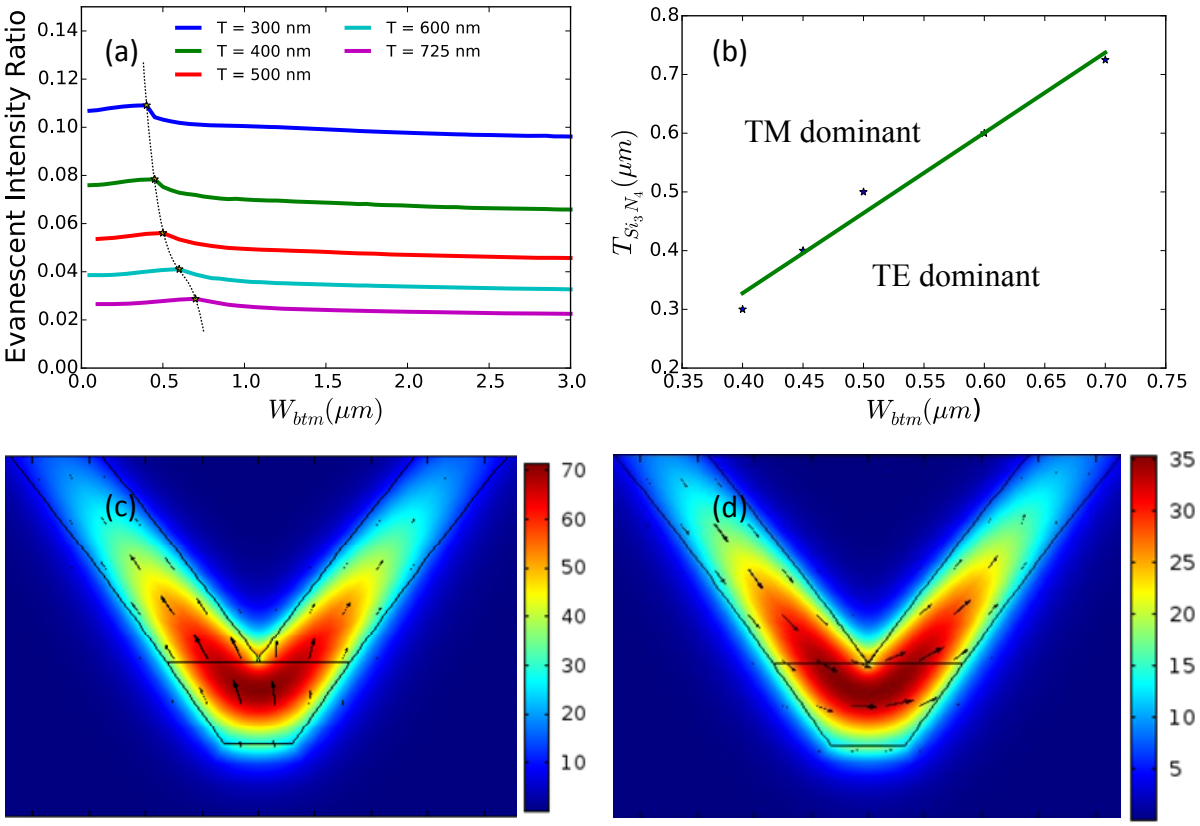

FIG. 3. (a) *EIR* as a function of W_{btm} and T at 1550 nm. The dotted line connects the peaks of the curves. (b) The waveguide thickness T as a function of *EIR* peak location. (c) The mode profile of the waveguide with W_{btm} = 0.6 μm and T = 725 nm. The black arrows indicate the electrical field orientation. (d) The mode profile of the waveguide with W_{btm} = 0.65 μm and T = 725 nm. The black arrows indicate the electrical field orientation.

3.2 Mode distribution

The dotted line in FIG. 3(a) serves as a good boundary to differentiate the TE and the TM modes. If we record the peak locations and the corresponding waveguide thicknesses, the relation between T and W_{btm}, shown in FIG. 3 (b), illustrates the boundary more intuitively. Linear curve fitting reveals the boundary function to be

$$T_{Si_3N_4} = 1.366 W_{btm} - 0.2192 \quad (2)$$

For a given waveguide, when W_{btm} is narrower than the peak location predicted in FIG. 3(b), the fundamental TM mode ($E_{11}y$) is dominant, and higher order TM modes and TE modes are leaky. The mode index of $E_{11}y$ has the maximum value when W_{btm} is around 0.2 μm. Then it decreases as the waveguide becomes wider. The reason for the mode index drop is that the TM mode is less tightly guided and more energy extends into the cladding region. This also explains the increase of *EIR* in FIG. 3(b). When W_{btm} is approaching the peak location, the imaginary part of the mode index is sufficiently large ($> 2\times10^{-10}$) such that we don't include the data in the plot. Thus there is discontinuity between $E_{11}y$ and $E_{11}x$ mode indices.

When W_{btm} is larger than the peak location, the fundamental TE mode ($E_{11}x$) is dominant, and the TM mode is neglected in this case. Higher order TE mode will tail into the Si_3N_4 side walls and leak into the slab region, if the waveguide is not

sufficiently wide. However, as the waveguide becomes wider, higher order TE modes emerge (FIG. 4(d) and (e)). The starting point of $E_{21}x$ mode, circled by the purple dashed line (FIG. 4(a)), is defined when the imaginary part of the mode index is negligibly small ($< 2\times10^{-10}$). If waveguide width is smaller than the starting point of its $E_{21}x$ mode, the waveguide can be viewed as a single mode waveguide that supports $E_{11}x$ mode dominantly. The starting point of $E_{21}x$ mode differs for waveguides with different thicknesses. The relation between the starting points of the $E_{21}x$ modes and waveguide thicknesses T is linearly curve fitted as

$$T_{Si_3N_4} = 0.1734W_{btm} + 0.2461 \tag{3}$$

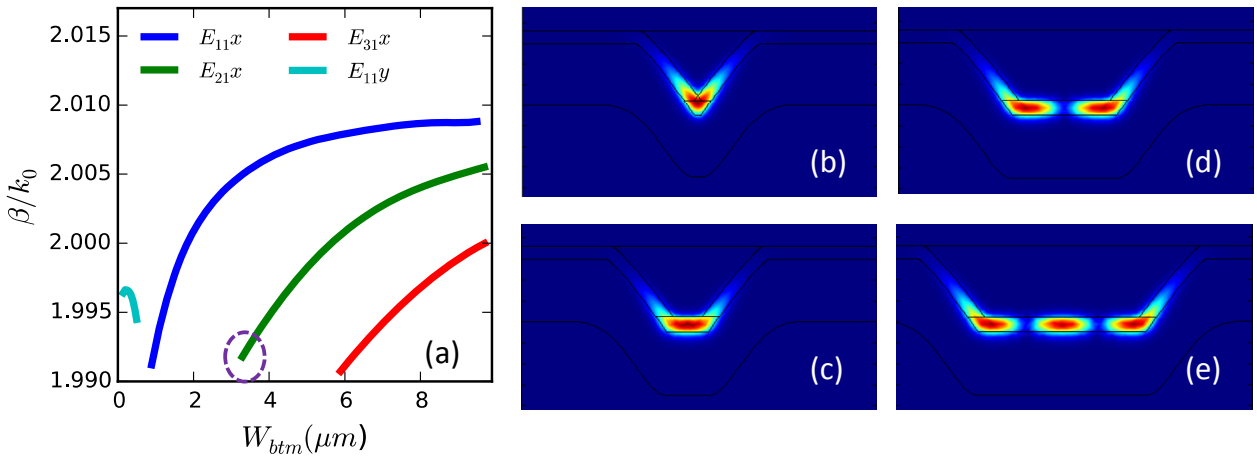

FIG. 4. (a) Mode indices as a function of W_{btm} for a given waveguide with T = 725 nm at 1550 nm. (b) $E_{11}y$ mode profile at W_{btm} = 0.3 μm. (c) $E_{11}x$ mode profile at W_{btm} = 2 μm. (d) $E_{21}x$ mode profile at W_{btm} = 5 μm. (e) $E_{31}x$ mode profile at W_{btm} = 8 μm. The purple circle in (a) indicates the starting point of a steady $E_{21}x$ mode.

By combining Eq. (2) and Eq. (3), the boundary map for TE and TM modes, the TE single mode and the TE multimode can be plotted in one figure.

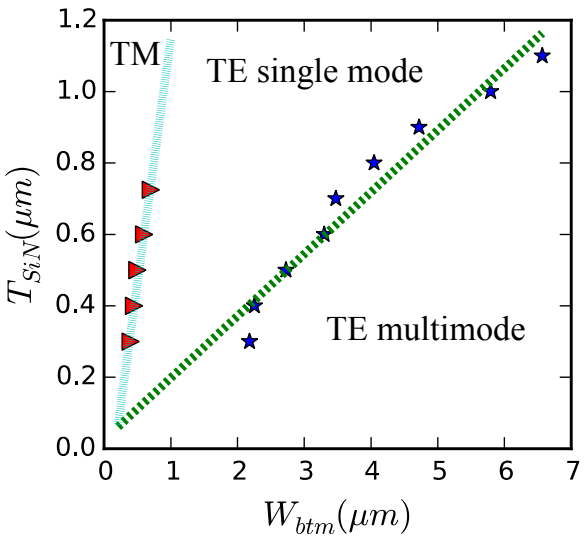

FIG. 5. Boundary map for the TM and the TE modes, and the TE single mode and the TE multimode for waveguide with etching depth H = 3.5 μm at 1550 nm. The red triangles represent the peak locations in *EIR* figure. The blue stars represent the starting points in FIG.4 (a).

3.3 Waveguide dispersion

Si_3N_4 waveguides can be used in nonlinear applications, in which phase matching is critical to broadband wavelength conversion. Therefore, dispersion should be engineered by manipulating the waveguide geometries so that the pump wavelength is in the anomalous region and close to the zero dispersion wavelength (ZDW). One way to shift the ZDW and maintain high mode confinement is to increase Si_3N_4 thickness [23]. However, this method needs special care during fabrication to avoid film cracking. The Si_3N_4 layer thicknesses are usually limited to 400 nm before tensile stress causes cracks on the film [24]. Fabricating thicker waveguides requires annealing and the recipe may differ for different film thicknesses. Another way to operate the waveguide dispersion is to change the waveguide width, which is much easier to achieve in fabrication. This is shown in FIG.6, where we plot the calculated dispersion parameter D as a function of wavelength for the waveguides with fixed thickness T = 725 nm and four different widths W_{btm}, ranging from 0.2 μm to 5 μm. The bulk Si_3N_4 dispersion parameter, derived from Sellmeire equation in [6], is also shown as a comparison.

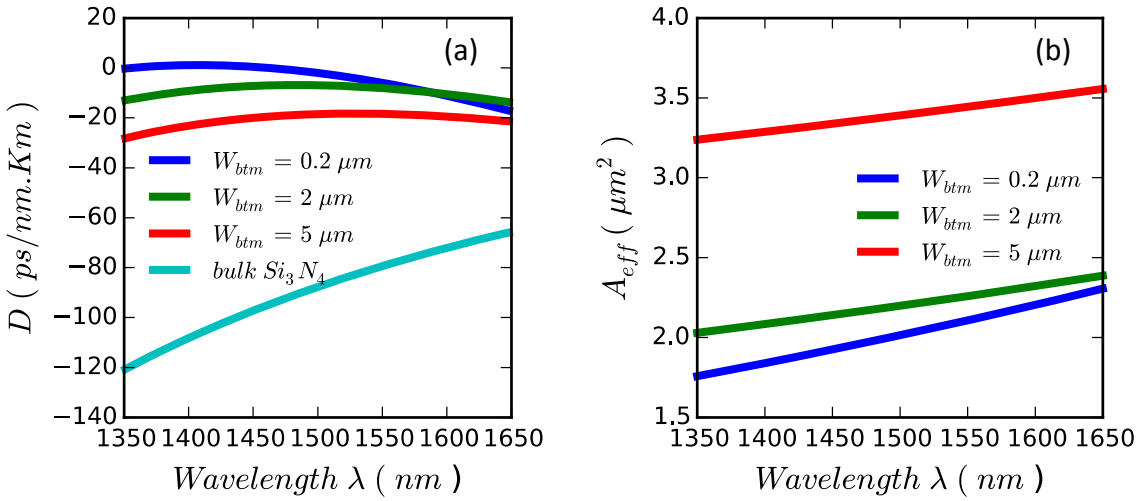

FIG. 6. (a) Dispersion parameter *D* for bulk Si_3N_4 (Cyan) and waveguides with a fixed thickness 725 nm and bottom waveguide width W_{btm} of 0.2 μm (blue), 2 μm (green) and 5 μm (red). The waveguide with W_{btm} 0.2 μm has two ZDWs, 1356 nm and 1462 nm. The other two waveguides and bulk Si_3N_4 have no ZDW. (b) The effective mode area of the waveguides as a function of wavelength and waveguide width.

All three waveguides have dispersion parameter $|D| < 100$ ps/nm.Km. While bulk Si_3N_4 and wider waveguides (W_{btm} = 2 μm and W_{btm} = 5 μm) have no ZDW, the waveguide that support a quasi-TM mode (W_{btm} = 0.2 μm) has two ZDWs which are 1356 nm and 1462 nm. This waveguide dispersion remains almost flat in the range between 1356 nm and 1462 nm, indicating promising usage in supercontinumm generation, solitons, etc. Besides, its effective mode area is the smallest among all three waveguides, indicating tight mode confinement. Therefore, narrow waveguides that support a quasi-TM mode are suitable for nonlinear applications.

4. CONCLUSIONS

In conclusion, we have shown the numerical analysis of silicon nitride trench waveguides with etching depth of 3.5 μm. The analysis reveals the TM and TE mode boundary with respect to waveguide geometry parameters W_{btm} and T. The TE single mode and TE multimode boundary is also studied by recording the starting points of $E_{21}x$ modes. Dispersion parameters and mode areas are plotted as a function of wavelength for waveguides with fixed thickness T = 725 nm. A narrow waveguide supporting a quasi-TM mode has ZDWs and a smaller mode area. It is therefore a good candidate for nonlinear integrated photonics.

The study presented above is of practical meaning in designing applications for silicon nitride trench waveguides. For example, the study of mode distribution can be used to facilitate coupling light into antenna in sensing applications,

while the study of dispersion parameter will provide guidance in nonlinear applications. With the help of the mode analysis, we believe the silicon nitride trench waveguide will find more applications.

5. ACKNOWLEDGMENT

This work is supported by a grant of the National Science Foundation ECCS 1449397 SNM.

REFERENCES

[1] S. Romero-García, F. Merget, F. Zhong, H. Finkelstein, and J. Witzens, "Silicon nitride CMOS-compatible platform for integrated photonics applications at visible wavelengths," *Opt. Express*, vol. 21, no. 12, p. 14036, Jun. 2013.

[2] C. H. Henry, R. F. Kazarinov, H. J. Lee, K. J. Orlowsky, and L. E. Katz, "Low loss Si3N4?SiO2 optical waveguides on Si," *Appl. Opt.*, vol. 26, no. 13, pp. 2621–2624, Jul. 1987.

[3] M. Melchiorri, N. Daldosso, F. Sbrana, L. Pavesi, G. Pucker, C. Kompocholis, P. Bellutti, and A. Lui, "Propagation losses of silicon nitride waveguides in the near-infrared range," *Appl. Phys. Lett.*, vol. 86, no. 12, p. 121111, Mar. 2005.

[4] A. Melloni, F. Morichetti, R. Costa, G. Cusmai, R. G. Heideman, R. Mateman, D. H. Geuzebroek, and A. Borreman, "TriPleX: A new concept in optical waveguiding," in *13th Eur. Conf. Integrated Optics (ECIO), Copenhagen, Denmark*, 2007.

[5] J. F. Bauters, M. J. R. Heck, D. John, D. Dai, M.-C. Tien, J. S. Barton, A. Leinse, R. G. Heideman, D. J. Blumenthal, and J. E. Bowers, "Ultra-low-loss high-aspect-ratio Si3N4 waveguides," *Opt. Express*, vol. 19, no. 4, pp. 3163–3174, Feb. 2011.

[6] Y. Huang, Q. Zhao, L. Kamyab, A. Rostami, F. Capolino, and O. Boyraz, "Sub-micron silicon nitride waveguide fabrication using conventional optical lithography," *Opt. Express*, vol. 23, no. 5, p. 6780, Mar. 2015.

[7] D. J. Moss, R. Morandotti, A. L. Gaeta, and M. Lipson, "New CMOS-compatible platforms based on silicon nitride and Hydex for nonlinear optics," *Nat. Photonics*, vol. 7, no. 8, pp. 597–607, Aug. 2013.

[8] K. Ikeda, R. E. Saperstein, N. Alic, and Y. Fainman, "Thermal and Kerr nonlinear properties of plasma-deposited silicon nitride/ silicon dioxide waveguides," *Opt. Express*, vol. 16, no. 17, p. 12987, Aug. 2008.

[9] J. S. Levy, A. Gondarenko, M. A. Foster, A. C. Turner-Foster, A. L. Gaeta, and M. Lipson, "CMOS-compatible multiple-wavelength oscillator for on-chip optical interconnects," *Nat. Photonics*, vol. 4, no. 1, pp. 37–40, Jan. 2010.

[10] T. Herr, K. Hartinger, J. Riemensberger, C. Y. Wang, E. Gavartin, R. Holzwarth, M. L. Gorodetsky, and T. J. Kippenberg, "Universal formation dynamics and noise of Kerr-frequency combs in microresonators," *Nat. Photonics*, vol. 6, no. 7, pp. 480–487, Jul. 2012.

[11] A. R. Johnson, Y. Okawachi, J. S. Levy, J. Cardenas, K. Saha, M. Lipson, and A. L. Gaeta, "Chip-based frequency combs with sub-100 GHz repetition rates," *Opt. Lett.*, vol. 37, no. 5, p. 875, Mar. 2012.

[12] R. Halir, Y. Okawachi, J. S. Levy, M. A. Foster, M. Lipson, and A. L. Gaeta, "Ultrabroadband supercontinuum generation in a CMOS-compatible platform," *Opt. Lett.*, vol. 37, no. 10, p. 1685, May 2012.

[13] Q. Zhao, Y. Huang, C. Guclu, F. Capolino, and O. Boyraz, "Optical Leaky Wave Antenna Experiment Demonstration and Electronic Modulation Investigation," in *CLEO*, 2015, p. JTh2A.43.

[14] Q. Zhao, C. Guclu, Y. Huang, S. Campione, F. Capolino, and O. Boyraz, "Experimental demonstration of directive Si3N4 optical leaky wave antennas with semiconductor perturbations at near infrared frequencies," in *Proc. SPIE 9365, Integrated Optics: Devices, Materials, and Technologies XIX*, 2015, vol. 9365, p. 93651K–93651K–10.

[15] Q. Zhao, C. Guclu, Y. Huang, F. Capolino, and O. Boyraz, "Plasmon Optical Trapping in Silicon Nitride Trench Waveguide," in *CLEO: Science and Innovations*, 2015, p. JTu5A–80.

[16] Y. Huang, Q. Zhao, N. Sharac, R. Ragan, and O. Boyraz, "Highly nonlinear sub-micro silicon nitride trench waveguide coated with gold nanoparticles," in *SPIE*, 2015, vol. 9503, p. 95030H–95030H–8.

[17] P. M. Pelosi, P. Vandenbulcke, C. D. W. Wilkinson, and R. M. De La Rue, "Propagation characteristics of trapezoidal cross-section ridge optical waveguides: an experimental and theoretical investigation," *Appl. Opt.*, vol. 17, no. 8, pp. 1187–1193, Apr. 1978.

[18] J. G. Gallagher, "Mode dispersion of trapezoidal cross-section dielectric optical waveguides by the effective-index method," *Electron. Lett.*, vol. 15, no. 23, pp. 734–736, Nov. 1979.

[19] T. Miyamoto, "Numerical analysis of a rib optical waveguide with trapezoidal cross section," *Opt. Commun.*, vol. 34, no. 1, pp. 35–38, Jul. 1980.

[20] G. Yue-Jin, L. De-Jun, and A. D. Klemm, "Numerical investigation of a trapezoidal cross-section ridge optical waveguide," *Numer. Methods Partial Differ. Equ.*, vol. 12, no. 3, pp. 307–314, May 1996.

[21] Y. Huang, *Integrated optical signal processing based on optical waveguides and wavefront-engineered planar devices*. Irvine, Calif: University of California, Irvine, 2014.

[22] I. H. Malitson, "Interspecimen Comparison of the Refractive Index of Fused Silica," *J. Opt. Soc. Am.*, vol. 55, no. 10, p. 1205, Oct. 1965.

[23] J. P. Epping, M. Hoekman, R. Mateman, A. Leinse, R. G. Heideman, A. van Rees, P. J. M. van der Slot, C. J. Lee, and K.-J. Boller, "High confinement, high yield Si3N4 waveguides for nonlinear optical applications," *Opt. Express*, vol. 23, no. 2, pp. 642–648, Jan. 2015.

[24] K. Luke, A. Dutt, C. B. Poitras, and M. Lipson, "Overcoming Si_3N_4 film stress limitations for high quality factor ring resonators," *Opt. Express*, vol. 21, no. 19, p. 22829, Sep. 2013.